2013

Dynamics at a Janus interface

M. von Domaros

D. Bratko
Virginia Commonwealth University, dbratko@vcu.edu

B. Kirchner

A. Luzar

Dynamics at a Janus interface

Michael von Domaros,[†,‡] Dusan Bratko,[†] Barbara Kirchner,[‡] and Alenka Luzar[*,†]

Virginia Commonwealth University, Richmond, VA, USA, and Universität Leipzig, Leipzig, Germany

[*]To whom correspondence should be addressed
[†]Virginia Commonwealth University
[‡]Universität Leipzig

Abstract

Electric field effects on water interfacial properties abound, ranging from electrochemical cells to nanofluidic devices to membrane ion channels. On the nanoscale, spontaneous orientational polarization of water couples with field alignment, resulting in an asymmetric wetting behavior of opposing surfaces – a field-induced analog of a chemically generated *Janus* interface. Using atomistic simulations, we uncover a new and significant field polarity (sign) dependence of the dipolar-orientation polarization *dynamics* in the hydration layer. Applying electric fields across a nanoparticle, or a nanopore, can lead to close to two orders of magnitude difference in response times of water polarization at opposite surfaces. Typical time scales are within the $O\left(10^{-1}\right)$ to $O\left(10\right)$ picosecond regime. Temporal response to the field change also reveals strong coupling between local polarization and interfacial density relaxations, leading to a nonexponential and in some cases, nonmonotonic response. This work highlights the surprisingly strong asymmetry between reorientational dynamics at surfaces with incoming and outgoing fields, which is even more pronounced than the asymmetry in static properties of a field-induced Janus interface.

Introduction

Trends towards miniaturization over the last decades and the recent advent of nanotechnology have provided new challenges for researchers in materials science, engineering, and biomimetic chemistry. Reducing the size of the system enables the integration of many processes into a single device, increasing performance and productivity. The high surface-to-volume ratio in nanodevices makes the control and functionalization of surfaces a dominating factor in their design. A promising technique to modify the interfacial characteristics is electrowetting,[1] which has already been exploited in numerous applications, e.g. in microfluidics, ink-jet printing, or electric control of optical properties.[2–8] Switching from hydrophobic to hydrophilic states via electrowetting has also been suggested as a mechanism for voltage-gated water and ion flow through nanochannels.[9–11] Furthermore, the interplay between electromagnetic fields and nanoscopic water layers and their

manipulation is discussed in the medical sciences as a factor in photobiomodulation, also known as low-level laser therapy.[12,13]

The basic thermodynamic theory of electrowetting predicts a reduction in contact angle θ_c,[1,2] and an increase in pressure and density[14] upon application of an electric field, depending only on the strength of the field. Concepts of macroscopic surface thermodynamics are, however, not sufficient to describe new phenomena observed at the nanoscale and experiments become increasingly challenging.[15] Atomistic simulations, on the other hand, are ideally suited for studies in the nanoscale regime.[16] Using this approach, we have shown that, when surface-to-bulk fractions are high enough, electrowetting in a nanopore depends on field direction and polarity.[17] A field-induced crossover from drying to wetting behavior is a general feature in hydrophobic nanopores, but will occur at lower field strengths when the field is aligned parallel to the interface rather than perpendicular.[17–19] In an electric field $\mathbf{E}$ perpendicular to the interface, spontaneous orientational polarization of water, associated with interfacial hydrogen bonding, competes with the field alignment (measured in terms of the field-induced overall dipole moment $\mathbf{M}$), resulting in an asymmetric behavior of opposing surfaces. Wetting ability is quantified in terms of wetting free energy $\Delta\gamma = \gamma_{\mathrm{sl}} - \gamma_{\mathrm{sv}} = \gamma\cos\theta_c$, where $\gamma_{\alpha\beta}$ denotes the interfacial free energy between phases α and β, and subscripts s, l, and v refer to the solid, liquid, and vapor phase, respectively. Since water is easier to polarize along the outgoing (E_{out}) than the incoming field (E_{in}), the reduction of the wetting free energy, which is dominated by the term $-\mathbf{E}\cdot\mathbf{M}$, is bigger for the field with outgoing direction, and $\Delta\gamma(E_{\mathrm{out}}) < \Delta\gamma(E_{\mathrm{in}})$. By carefully tuning the field strength, a Janus interface[20] emerges,[16–19] with water favorably attracted to one surface (hydrophilic), but abhorred on the other (hydrophobic). Thus, in a chemically uniform system a wetting asymmetry is induced solely by applying an electric field.[16–19]

These observations suggest a general way to control electrowetting in nanoporous materials, with main determinants being not only field strength but also its direction and polarity. Recently, excellent reports have been published on changing the macroscopic water contact angle by altering the surface polarity or morphology by various methods.[21–23] The slow switching time (hours

or days)[21] and hysteresis,[22] however, pose current experimental challenges. Switchable wettability/hydrophobicity[24,25] due to electrowetting suggests an exciting alternative. For faster actuation, descent to nanoscale is an essential advantage with a promise of immediate, hysteresis-free response.

In general, the response to the change in applied field can take place in two partially overlapping stages characterized by distinct time scales. The first stage involves water polarization and concomitant change in the interfacial free energy. Depending on the system in question, this stage can be followed by a slower process of solvent transfer toward a new equilibrium state associated *e.g.* with a change in droplet spreading, nanopore wetting, electrostriction, or nanoparticle reorientation.[16,26] In this article, we focus on the initial stage involving fast dynamics of *interfacial* polarization, and local density adjustments in response to the imposition of the field. Wile dielectric response of water includes significant quadrupolar and higher multipole contributions to the overall polarization,[27] we concentrate on the dipole-orientation contribution. We do not address weak electronic-polarization effects in this study. Our results for interfacial water emphasize a remarkable dependence of the polarization *dynamics* on the direction of the field. In a window of applied field strengths, dielectric relaxation at the interface can be over 25 times faster than in the bulk aqueous phase.

Since a field-induced Janus interface can only be obtained when walls are initially hydrophobic, we concentrate on this situation. Nanoelectrowetting will, however, generally depend on field direction. We therefore include molecular simulation results for polarization dynamics in confinements between hydrophilic walls in the Supporting Information (SI). By doing so, we uncover the pronounced asymmetry in polarization *dynamics* even when static properties do not show *Janus* behavior.

The remainder of this article is organized as follows. After describing the models and systems, we discuss how the competition between orientational preferences and field alignment leads to the polarity dependence of static and dynamic quantities of interfacial water. We study dipole angle distributions, fluctuation dynamics of interfacial water polarization, and the dynamic response to

the imposition of the field. We show additional data in support of our conclusions in the SI. Finally, we summarize our findings and outline future work.

Models and Methods

Our model system consists of a slab of 839 water molecules, confined between two parallel walls structured like a graphite bilayer and separated by a distance $D = 28.6\,\text{Å}$ (Figure 1). This distance has been found sufficient to secure convergence with respect to D for interfacial properties we study.[17,19] The walls consist of 767 carbon-like atoms, which are held at fixed positions during the simulation.

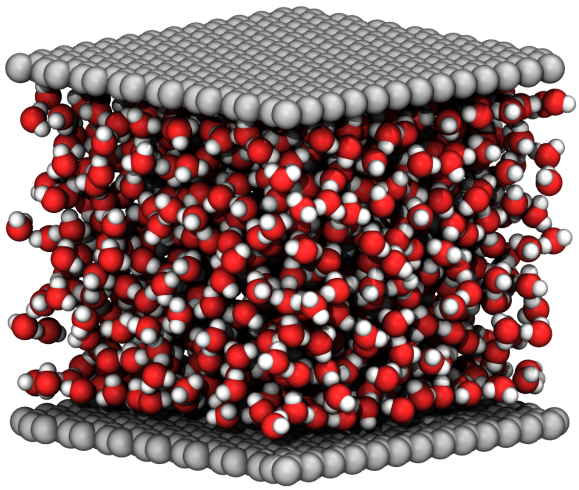

Figure 1: Random snapshot of the system without an electric field. Applying periodic boundary conditions renders confinement walls twice as thick (bilayer of graphene).

Water–wall interactions were taken from Werder et al.,[28] corresponding to microscopic contact angles[29–31] of either 128°, or 70°. In the present text, we refer to the former as hydrophobic and the latter as hydrophilic. Note that we only consider systems where both walls are chemically equal. Asymmetries arise only after imposition of the electric field.

Water molecules are described by the extended simple point charge (SPC/E) model,[32] which has already been used successfully in similar studies.[16–19,26,33,34] We note that the choice of a particular force field may introduce some quantitative differences in orientational preferences of water

near interfaces, but angle preferences due to anisotropic hydrogen bond interactions are a common and well-reproducible feature in a variety of models including ST2,[35] TIP4P,[36] and SPC/E.[31] The application of electric fields may suggest the use of electronically polarizable, and possibly reactive force fields to account for electronic polarization and dissociation due to electric fields. However, fields of up to $0.1\,\mathrm{V\,\AA^{-1}}$ do not significantly polarize water molecules,[37] and cannot decompose them when the flow of electric current is prevented.[38] With all components of molecular polarizability of water close to $1.5\,\mathrm{\AA^3}$,[39] the above fields can induce a change in dipole moment of water only up to 0.2 %. According to recent studies, only fields exceeding the dissociation threshold of $\sim 0.3\,\mathrm{V\,\AA^{-1}}$ are able to significantly dissociate water molecules.[40,41] Although Liu et al. observed interesting effects of molecular polarizability on aqueous interfacial diffusion,[42] we note that translation is not directly coupled to the rapid polarization response we study. The water model we use also quantitatively affects the Debye relaxation time τ_D, which is related to the correlation time τ_M of the collective dipole moment relaxation function $\langle \mathbf{M}(t)\cdot\mathbf{M}(0)\rangle / \langle M^2(0)\rangle$.[43–45] The equality holds if Ewald summation with conducting boundary conditions is used; for non-conducting boundary conditions or a different treatment of long-range electrostatic interactions, however, τ_M needs to be scaled appropriately.[44,45] Literature values for τ_D range between 5 and 10 ps for SPC/E water depending on the simulation methodology.[45–48]

Molecular dynamics simulations are performed in the canonical ensemble at $T = 300\,\mathrm{K}$ using the LAMMPS package.[49] Lennard–Jones interactions and real-space Coulomb forces are cut off beyond 11 Å. Thermostating is achieved by a Nosé–Hoover thermostat with a 100 fs time constant. The simulation box is a rectangular prism with edges $L_x = 31.9\,\mathrm{\AA}$, $L_y = 31.2\,\mathrm{\AA}$, and $L_z = 31.9\,\mathrm{\AA}$. Periodic boundary conditions are applied in all three dimensions. Equilibrated systems are typically simulated for $\sim$ 16.8 ns with a 1 fs time step. Electric fields $\mathbf{E}$ of selected input strengths in the range from 0.01 to $0.1\,\mathrm{V\,\AA^{-1}}$ ($\mathbf{E}$ replacing the common notation $\mathbf{E}_0$[17,50–52]) are applied perpendicular to the walls. While the actual fields depend on the position, the fixed values $\mathbf{E}$ correspond to a set of displacement fields[27], $\mathbf{D}_z$, which (unlike $\mathbf{E}_z(z)$) are independent of the position. Since we use conducting ("tin foil") boundary conditions, the actual fields in the bulk-like phase beyond

$\sim 0.5\,\mathrm{nm}$ away from the surfaces are close to the input strengths $\mathbf{E}$. The reader is referred to ref. 27 for an in-depth description of the theoretical framework for the dielectric response in terms of the above field functions, and the results for the distance dependence of $\mathbf{E}_z(z)$ in the interfacial layer in closely related model systems. We follow the IUPAC definition of the dipole moment, where the vector points from negative to positive charges.

Results and discussion

Orientational preferences and field alignment

It is well known, that the molecular asymmetry, and anisotropic hydrogen bond interactions of water result in an orientational bias near interfaces.[35,36,53–55] In order to optimize the hydrogen bond network, water dipoles align almost parallel to the surface, pointing just slightly away, and leading to spontaneous polarization near the interface.[54] We quantify the dipole contribution to the interfacial polarization in terms of the total interfacial dipole moment $\mathbf{M}(t) = \sum_i^N \mu_\mathbf{i}(t)$, which is the sum over all N water dipoles $\mu_\mathbf{i}$ in the first hydration layer. We define this layer as the region between the wall and the first minimum in water density (determined through the density layer profiles, section SI-1). At two identical, opposing surfaces, and in the absence of an applied field, the average dipole contributions to polarization $\langle M(t)\rangle$ will be of the same magnitude, but point in opposite directions. Consequently, average values of

$$\cos\varphi(t) = \frac{\mathbf{M}(t)\cdot\mathbf{e_z}}{M(t)}, \tag{1}$$

the cosine of the angle between $\mathbf{M}(t)$ and $\mathbf{e_z}$, a unit vector perpendicular to the walls, will be of opposite sign. Figure 2 shows these averages $\langle\cos\varphi(t)\rangle$. Upon application of perpendicular external electric field, water dipoles at both walls gradually align with the direction of the field. Since the initial orientational preferences are opposite, the alignment with the field competes with the orientational bias if the electric field is incoming (red lines) and water hydrogens are pushed

towards the surface, but cooperates with it when the electric field is outgoing (purple lines) and water hydrogens are turned away from the wall. As a result, the orientational term in polarization shifts in the direction of the field but remains asymmetric. This asymmetry is shown schematically on the right-hand side of Figure 2. Sensitivity to the field is gradually diminishing with increasing field strengths, and saturation seems to occur at fields slightly above $0.1\,\mathrm{V\,\AA^{-1}}$, but these high field strengths were not investigated further.

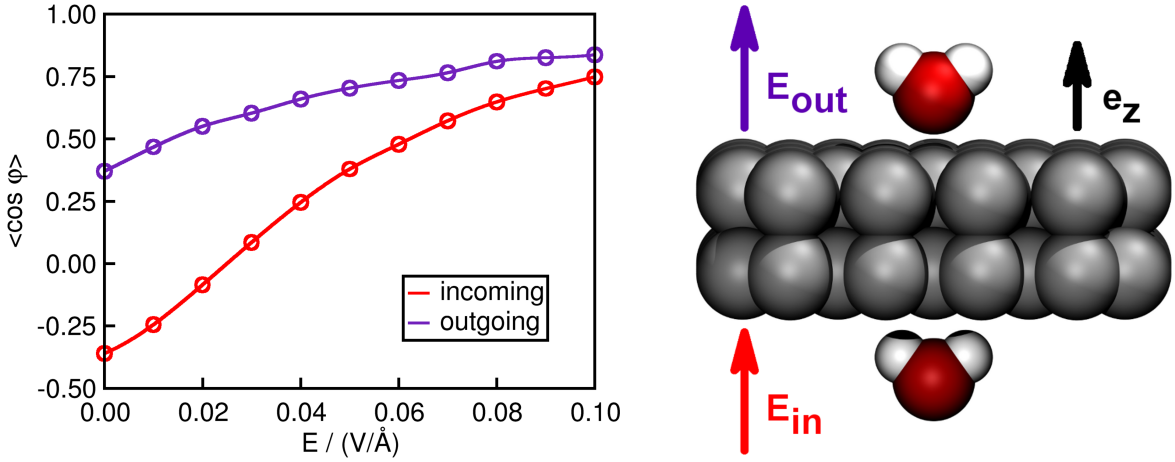

Figure 2: Left: Field dependence of $\langle\cos\varphi\rangle$, where φ is the angle between the overall interfacial dipole moment and the electric field $\mathbf{E}$ parallel to $\mathbf{e_z}$, where $\mathbf{e_z}$ is a unit vector perpendicular to the interface. Right: Scheme demonstrating the asymmetric behavior of interfacial water molecules subject to incoming (E_{in}) and outgoing (E_{out}) fields.

It has been demonstrated in simulations that such a high alignment of water dipoles can be achieved without serious penalties in hydrogen bond number and free energies, and without distortion of tetrahedral coordination.[34,56–61] We also found no significant change in the local tetrahedral order parameter[62] and in oxygen triplet distributions[34] in our systems.

We note that the field strength at which *incoming* fields roughly compensate the angular bias of the hydrogen bonds at the interface, i.e. where $\langle\cos\varphi\rangle \sim 0$, is slightly below $0.03\,\mathrm{V\,\AA^{-1}}$. These fields are comparable to fields in ion channels[52] and ionic colloids,[63,64] but are an order of magnitude weaker than local fluctuating fields present in liquid water and solution.[65] We obtain very similar results for hydrophilic walls (section SI-2), however, since stronger water–wall interactions must be overcome in hydrophilic systems, a slightly higher field strength is required to

achieve similar effects.

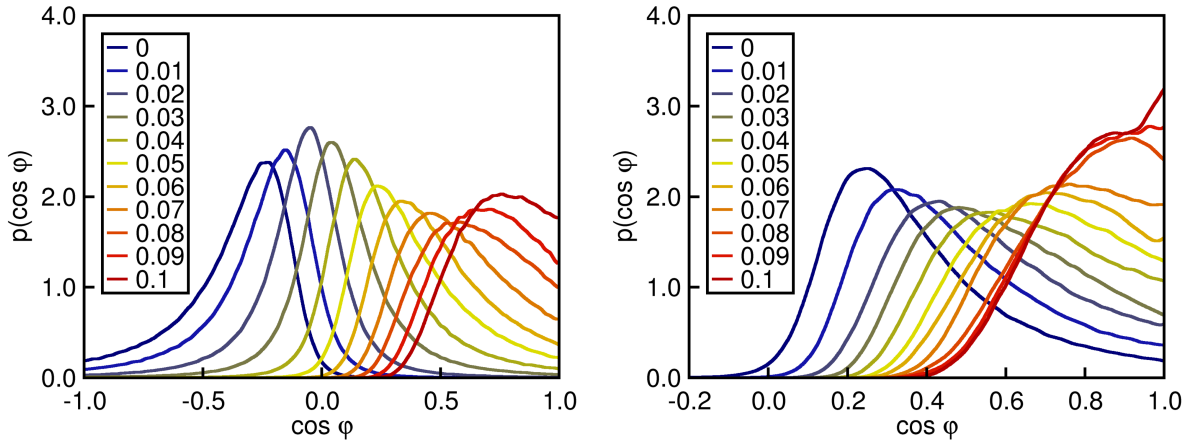

Figure 3: Dipole angle distributions $p(\cos\varphi)$ for all investigated field strengths and given system size. Left: incoming fields; right: outgoing fields. The color gradient (blue $\rightarrow$ yellow $\rightarrow$ red) indicates field strengths growing in increments of $0.01\,\mathrm{V\,\AA^{-1}}$ from 0 to $0.1\,\mathrm{V\,\AA^{-1}}$. Curves are normalized to unit area. Note the different $\cos\varphi$ scales.

To gain a more detailed picture of orientational polarization near the interface we show dipole angle distributions $p(\cos\varphi)$ in the hydrophobic system (Figure 3) and specified system size. The corresponding figures for the hydrophilic system can be found in section SI-2. The color gradient (blue $\rightarrow$ yellow $\rightarrow$ red) indicates growing field strengths. As already shown by looking at the average values (Figure 2), distributions are shifted systematically to higher values of $\cos\varphi$ with growing field strengths. The widths of the distributions however, behave differently. For incoming fields, they decrease until they are narrowest around $0.03\,\mathrm{V\,\AA^{-1}}$ and $\langle\cos\varphi\rangle \sim 0$, from where on they broaden again. For outgoing fields, the distributions broaden monotonically. These qualitative trends are robust with respect to system size and any variation due to size dependence[45] cancels out in normalized correlation functions. The restoring force which causes the decay of thermal fluctuations from the average orientation is strongest in systems with narrowest angle distributions, as manifested in the dynamic quantities we describe below.

It is important to note that the competition between orientational preferences and field alignment is a pure interfacial phenomenon. As such it becomes important on the nanoscale, where the fraction of interfacial molecules is significant. The range of surface effects is seen in Figure 4,

which shows probability distributions $p_z(\cos\varphi)$ evaluated at different positions z perpendicular to the interface in the field-free system (left) and under the influence of $E = 0.03\,\mathrm{V\,\AA^{-1}}$ (right). Dipole angle distributions are subject to the aforementioned angle preferences only at small distances from the interface. They are clearly unbiased in the middle part of the interface, which exhibits bulk-like behavior. In this domain, orientations are symmetrically distributed around $\cos\varphi \sim 0$, while they are visibly shifted within the solvation layers. To maintain the optimal angle relative to the walls on both sides, the angular shifts at the two walls, measured relative to a normal through the interface as a whole, are of opposite signs. An imposed electric field (Figure 4, right) affects the angle distributions at all positions, thus bringing the dipole orientations closer to the direction of the field. Within the interfacial layer on the lower wall, where the field is outgoing, the initially weak spontaneous orientational polarization is intensified. At the opposite wall, the incoming field tends to align water dipole against their spontaneous orientation, bringing the net dipole contribution to the polarization closer to zero. At even stronger fields than the one shown in Figure 4 (right), the alignment is dominated by the field, resulting in polarization contribution in the direction of the field on both walls.

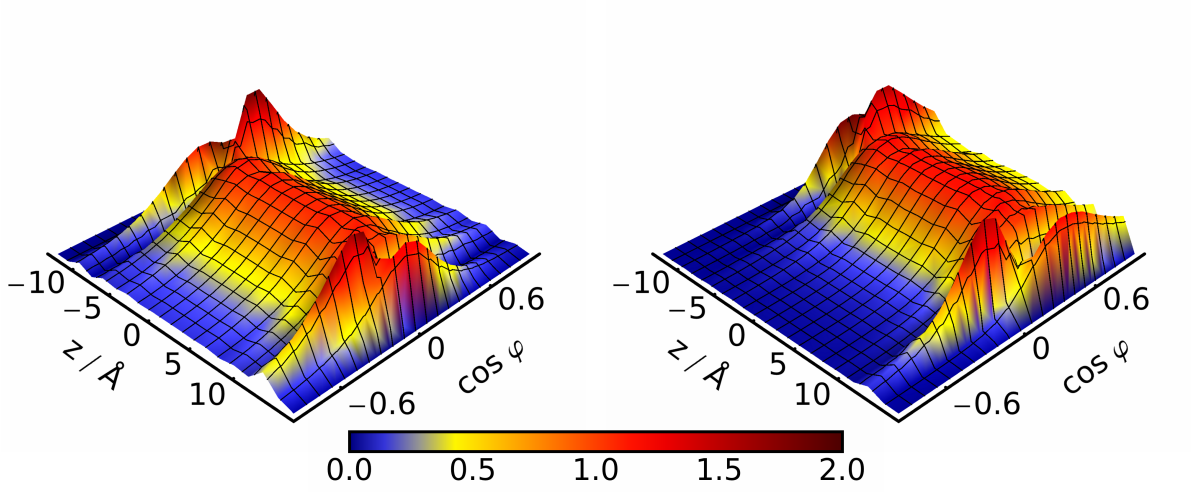

Figure 4: Probability distributions $p_z(\cos\varphi)$ as a function of z, the position perpendicular to the interfaces. For a given value of z, curves are normalized to unit area. Left: field-free; right: $E = 0.03\,\mathrm{V\,\AA^{-1}}$.

Fluctuation dynamics of interfacial water polarization

The asymmetric wetting behavior discussed above reflects the competition between spontaneous orientational polarization of interfacial water, and alignment along the applied field. As a result, water density within the first hydration layer is enhanced for incoming fields, but is decreased for outgoing ones. The changes in the density maxima in the first hydration layer are illustrated in Figure 5 (see also section SI-1). The observed asymmetry trends illustrated in Fig. S1 agree qualitatively with the differences between interfacial water density profiles in positive and negative perpendicular fields, reported in refs. 17,27. The differences in wall materials, imposed conditions, and field specification preclude a qualitative comparison. As we expect the same competition to affect polarization dynamics, we explore the influence of the field on the orientational time correlation function. Reorientation correlations are anisotropic next to surfaces.[55,66,67] For our purposes the z-component is of greatest interest, because it relates to the dielectric relaxation along the field direction. Thus we explore the orientational correlation function

$$C_{\varphi}(t) = \frac{\langle \delta\cos\varphi(t)\,\delta\cos\varphi(0)\rangle}{\langle \delta^2\cos\varphi(0)\rangle}, \tag{2}$$

where $\delta\cos\varphi(t) = \cos\varphi(t) - \langle\cos\varphi\rangle$ denotes fluctuations of $\cos\varphi(t)$, as defined in Eq. Eq. (1), around its time average $\langle\cos\varphi\rangle$. Since the leading electric field contribution to interfacial free energy is given by the relation

$$\Delta_E\Delta\gamma \;\sim\; -\langle EM\cos\varphi\rangle/A, \tag{3}$$

with $\Delta_E\Delta\gamma$ denoting the field-induced change in wetting free energy $\Delta\gamma$ and A the surface area, these time correlation functions describe the dynamic response of the interfacial free energy to small changes (linear regime) in the electric field.

Figure 6 (left) shows the decay of polarization fluctuations under the influence of an electric field $E = 0.03\,\mathrm{V\,\AA^{-1}}$. As $C_{\varphi}(t)$ describes a collective process that involves multiple coupled molecular processes, a simple monoexponential decay function should not be expected, which is indeed the case. All correlation functions exhibit a sharp initial drop for times $< 1\,\mathrm{ps}$ due to the

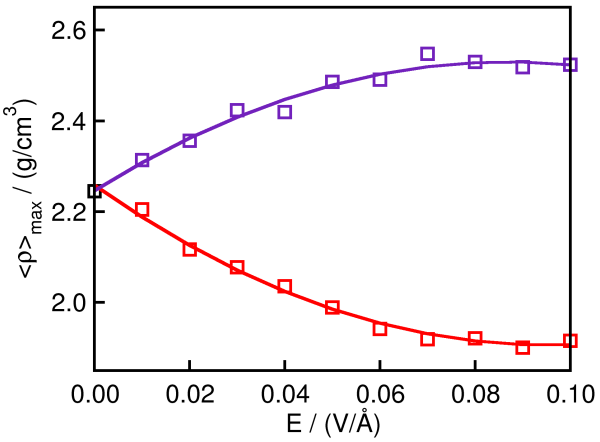

Figure 5: Maximum water density $\langle\rho\rangle_{\max}$ within the first hydration layer at various incoming fields E_{in} (red) and outgoing fields E_{out} (purple). Lines are to guide the eye.

coupling with fast molecular motions, such as vibrations and rotations (librational motions), and hydrogen bond dynamics.[68–72] After that the decay seems to be roughly exponential for intermediate times (the exact time interval depends on the field strength), however, significant curvatures on the semi-log plots can be seen for some curves (e.g. $0.03\,\text{V}\,\text{Å}^{-1}$, incoming, Figure 6). At large times, all functions deviate from an exponential decay. It is however hard to accumulate statistically accurate data at long times, so we do not interpret these deviations. Characteristic decay times for the different systems we consider can be obtained by integration of correlation functions. This requires fitting the correlation functions by expressions that allow analytic extrapolation to very long times. In our case, good fits and essentially identical correlation times follow from stretched exponentials or a linear combinations of three exponential terms. Statistical noise is, however, considerable as times get longer and we obtain essentially the same decay times but with better statistics by listing the times at which correlation functions have decayed to $1/e$. Without making specific assumptions regarding the form of the decay, we compare correlation times from both procedures in Figure 6 (right). The qualitative behavior we observe and especially the asymmetries in response times, are essentially the same no matter how times are determined. Fluctuations in the field-free system decay to $1/e$ within 2.0 ps. For comparison, our Debye relaxation time in bulk H_2O, which is related to the correlation time of $C_\varphi(t)$, is 5.4 ps, well within the range of reported literature values for the same water model.[45–48] The non exponential decay and time scales for

$C_\varphi(t)$ at the interface differ from the bulk ones for several reasons. First, in field free systems dielectric relaxation is isotropic. For interfacial water on the other hand, Lee and Rossky showed[66] that singling out the vector component perpendicular to the surface results in a faster decay at hydrophobic surfaces, characterized by weak specific interactions between water protons and the wall. Our calculations reveal a similar anisotropy. The difference between interfacial and bulk water dynamics[55,66,73] has also been demonstrated at the liquid/vapor interface. In a comparison between the reorientation dynamics in a $(H_2O)_{108}$-cluster, which contains a significant percentage of interfacial molecules, and bulk water, Saito and Ohmine showed[73] that the first order collective orientational relaxation is considerably faster in the cluster than in the bulk. Further, the decay is not exponential anymore.

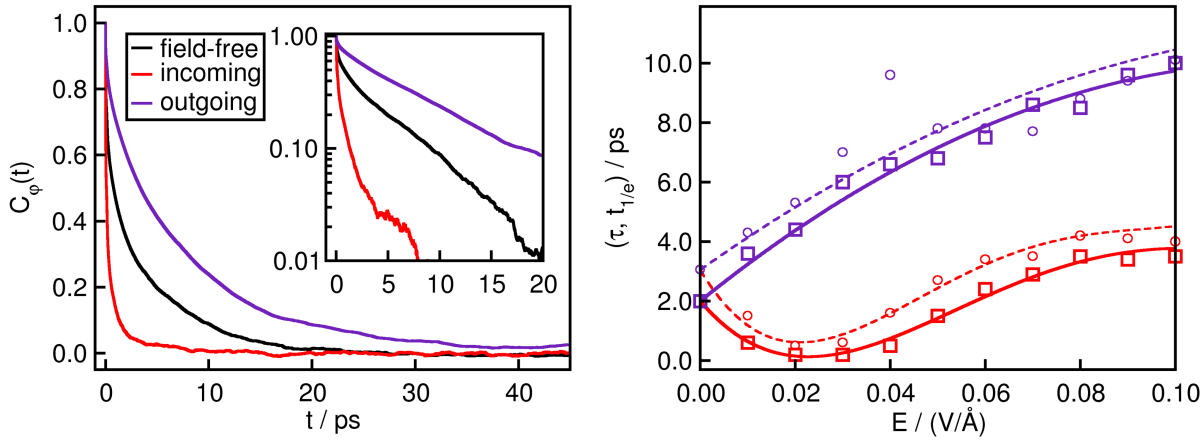

Figure 6: Left: Decay of polarization fluctuations in the field-free system (black) and for incoming (red) and outgoing (purple) fields of strength $E = 0.03\,\mathrm{V\,\AA^{-1}}$. The inset shows the same functions on a semi-logarithmic scale. Right: Characteristic time scales $t_{1/e}$ of the polarization fluctuation dynamics (squares, solid lines) and correlation times τ extracted by fitting a sum of three exponentials to correlation functions and subsequent integration (circles, dashed lines). Lines are to guide the eye.

At the hydrophilic walls, the first order orientational dynamics, characterized in terms of $C_\varphi(t)$, are somewhat slower (3.4 ps, see section SI-3), consistent with other simulations[55,66] and experiments[74] although in those works the second order anisotropy decay is investigated.

Imposition of an electric field results once again in asymmetries between incoming and outgoing fields: Fluctuations decay much faster, within $\sim$ 0.2 ps, when the electric field points towards

the surface; their decay is slowed down by close to two orders of magnitude ($\sim$ 6 ps), when the field points away. As shown in Figure 6 (right) the fastest decay of polarization fluctuations is observed at incoming field strengths around $0.03\,\mathrm{V\,\AA^{-1}}$, i.e. when the competition between orientational preferences and field alignment results in negligible water polarization. As illustrated in Figure 3 (left), this situation, achieved only in relatively weak incoming field, is characterized by the narrowest probability distribution over the angle of dipole alignment. On the wall, where the field is outgoing, on the other hand, the distribution over the angle monotonously broadens with strengthening the field. The restoring force causing the decay of eventual fluctuations from the average orientations is strongest at narrow angle distributions, hence the decay time monotonically increases in the layer under the outgoing field but passes through a minimum when the field is incoming. Past the minimum, the time scales get slower with increasing field on both surfaces. The asymmetries between incoming and outgoing field persist however, and we observe pronounced differences in decay rates even in our highest investigated field.

These findings resemble the results of recent molecular dynamics simulations[75] of Debenedetti and co-workers, where the authors investigated water in nanoscale confinement between β-cristobalite. By varying the surface electric charge through a linear scaling factor $k \in [0,1]$, which is similar to increasing an applied electric field, they observed a nonmonotonic dependence of both orientational and translational dynamics on k. A minimum in the relaxation times of the single molecule dipole time correlation function was found at about 60 % of the final charge, $k = 0.6$. It is plausible that both the behavior we illustrated in Figure 6 (right) and that reported in ref 75 have a common explanation in the balance between the angular bias due to hydrogen bonding and alignment by local electric field: In the state where the field balances the angle preferences of water, dipoles appear to orient least freely as angular distributions are narrowest in the vicinity of parallel dipole–wall orientation.

Dynamic response to the imposition of the field

Since the response of the system to our high electric fields is nonlinear (Figure 2), the time correlation functions presented in the previous section cannot be used to directly extract surface tension actuations rates via relation (Eq. Eq. (3)). Therefore we investigate the relaxation of $\cos\varphi(t)$ to its equilibrium value after switching the field from off to on. We calculate

$$R(t) = \frac{\overline{\delta\cos\varphi(t)}}{\overline{\delta\cos\varphi(0)}}, \tag{4}$$

where $\delta\cos\varphi(t)$ denotes the mean deviation of $\cos\varphi(t)$ from its equilibrium value under the influence of the field, and the time origin $t = 0$ is set at the time of the imposition of the field E. Overlined quantities denote averages over 1800 independent trajectories. Once again, for comparison purposes we estimate characteristic time scales in terms of the times where $R(t) = 1/e$ (Figure 7).

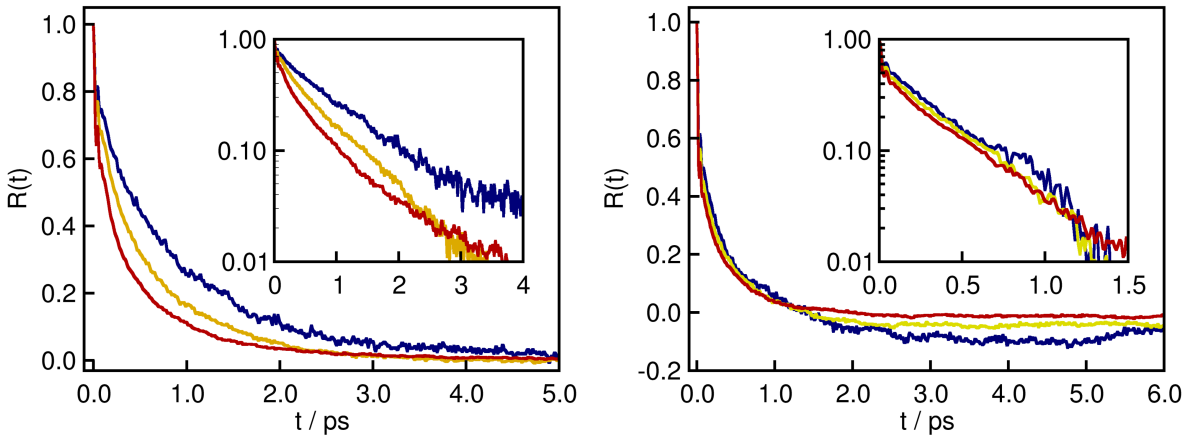

Figure 7: Relaxation of the dipolar-orientation polarization to its equilibrium value after switching the electric field from off to on. Field strengths are 0.03 (blue), 0.06 (yellow), and 0.09 V Å^{-1} (red). Left: incoming fields; right: outgoing fields.

In analogy with fluctuation dynamics (Eq. Eq. (2)), significant asymmetries arise between incoming and outgoing electric fields. Relaxation times decrease from 0.7 ps under the influence of an incoming electric field of 0.03 V Å^{-1} to 0.3 ps at 0.09 V Å^{-1}. Under the influence of outgoing fields, these times are of the order of 0.1ps and do not vary significantly with field strength. Re-

laxation times which we observe at these conditions are well below hydrogen bond lifetimes,[68–71] indicating that orientational ordering occurs without significant breaking of interfacial hydrogen bonds. This observation is consistent with reported resilience of the hydrogen bond network, which has been found surprisingly robust with respect to dielectric polarization.[34,56–61] What the above time scales do not reflect however, is the long time behavior of the relaxation functions. All curves for outgoing fields show a negative well starting at $\sim$ 1.5 ps and ending at $\sim$ 13 ps (section SI-3). This behavior is likely related to the adjustment of local density to the change of electric field, which we investigate in detail in section SI-4. Here, we will only summarize the main findings that are important to understand the effects in Figure 7. We study density fluctuation dynamics in the first hydration layer by calculating $C_N(t) \propto \langle \delta N(t)\, \delta N(0) \rangle$, where $\delta N(t)$ denotes the deviation of the number of molecules within the first hydration layer N from its time average $\langle N \rangle$. Density relaxes independently of the field direction within time scales of $\sim$ 1.2 ps, which is an order of magnitude slower than the response of polarization for outgoing fields (0.1 ps). When the electric field is switched on, the dipolar-orientation polarization overshoots, as it initially relaxes at the lower density corresponding to the absence of the field. As the density increases toward its equilibrium value, polarization retracts more slowly. The density adjustment is almost complete after $\sim$ 10 ps (section SI-1), which coincides with the end of the negative well shown in Figure S9. The disparity between the timescales of orientational and density relaxations is most prominent in the relatively weak field $E = 0.03\,\mathrm{V\,\AA^{-1}}$. Further, saturation effects in both the polarization (Figure 2) and density (Figure 5) reduce the relative sensitivity in stronger fields. Hence the negative minimum is most pronounced in weaker field.

The above mechanism has a smaller and *opposite* effect in incoming fields, which induce density depletion somewhat smaller than the density rise in the outgoing field (section SI-1). Since local density is decreased in this case, orientational polarization adjusts first to the higher density corresponding to zero field. Once density decreases to its equilibrium value, polarization follows. Retardations of similar magnitudes as the negative wells in outgoing fields are expected, this time however, in the positive direction (consistent with the data in Figure 7).

Concluding remarks and outlook

The competition between orientational polarization of water near interfaces and alignment of water dipoles with applied electric fields can result in distinctly different wetting behaviors of opposing surfaces, which we describe as a field-induced Janus interface. We investigated the local dynamics at such a Janus interface, which are an important criterion in the design of electro-switchable, fast response nanofluidic devices and may shed light on the function of biological voltage-gated channels.

Our Molecular Dynamics calculations uncovered a new and significant polarity dependence of the orientational time correlation function for interfacial water: when the electric field balances the angle preferences of water, dipoles can reorient least freely and relaxation times go through a minimum. Angle distributions are narrowest, indicating the biggest restoring force at these conditions. Only when the electric field is incoming do angle preferences and field alignment compete. When the electric field is outgoing, both effects cooperate resulting in monotonously increasing relaxation times; thus the asymmetric behavior at opposite confinement walls. The difference in response times is significant, with typical times in the $O\left(10^{-1}\right)$ to $O\left(10\right)$ picosecond regime. The peculiarly fast dynamics, achieved in a window of strengths of incoming electric field should reduce THz impedance of an aqueous nanofilm well below the value expected from bulk properties of water, a feature potentially detectable in dielectric spectroscopy experiments.[76,77]

While dielectric relaxation in bulk water decays monoexponentially, except for very short times, with an experimental relaxation time of $\sim$ 8 ps,[78,79] the interfacial relaxation functions show more complex behavior indicative of an interplay of molecular mechanisms. Competing effects of the field and spontaneous dipole alignments also explain the non monotonic dependence of orientational relaxation rates on the strength of the applied incoming field, a feature that can shed light on recent observations of a nonmonotonic change in water reorientation rate as a function of increasing solute polarity.[55,75] The existing analogy suggests the possibility of transitory tuning of interfacial dynamics by optimizing the external field as an alternative to permanent modulation that can be achieved by controlled chemical modification.

We also investigated hydration layer density dynamics, which are not affected by either field strength, or field direction. Typical response times to all fields are $\sim$ 1.2 ps. Density does however couple strongly to local polarization, as revealed by the temporal response of the system to electric fields. It will be interesting to see whether the dynamic response in polarization couples to hydrogen bond dynamics[42,80,81] as we have demonstrated to be the case for equilibrium values,[17,18] a question we will address in future work.

Acknowledgement

We thank Chris Daub for critical reading of the manuscript and Jihang Wang for his initial efforts. We acknowledge support from NSF (CHE-1213814) at early stage and DOE/BES (DE-SC-0004406) at final stage of the project. MvD thanks the German Academic Exchange Service and the German Science Foundation (KI-768/6-1) for travel support. This research used resources of the National Energy Research Scientific Computing Center (NERSC), which is supported by the Office of Science of the U.S. Department of Energy (DEAC02-05CH11231), and the Extreme Science and Engineering Discovery Environment (XSEDE), which is supported by NSF Grant No. OCI-1053575.

Supporting Information Available

Structure of water film under electric field. Structural and dynamic properties of water in a hydrophilic confinement. Density fluctuation dynamics. Includes nine graphs. This material is available free of charge via the Internet at `http://pubs.acs.org/`.

References

(1) Shapiro, B.; Moon, H.; Garrell, R. L.; Kim, C.-J. *J. Appl. Phys.* **2003**, *93*, 5794–5811.

(2) Mugele, F.; Baret, J.-C. *J. Phys.: Condens. Matt.* **2005**, *17*, R705–R774.

(3) Baret, J.-C.; Mugele, F. *Phys. Rev. Lett.* **2006**, *96*, 016106.

(4) Krupenkin, T.; Taylor, J. A.; Kolodner, P.; Hodes, M. *Bell Labs Tech. J.* **2005**, *10*, 161–170.

(5) Chen, J. Y.; Kutana, A.; Collier, C. P.; Giapis, K. P. *Science* **2005**, *310*, 1480–1483.

(6) Berge, B.; Peseux, J. *Eur. Phys. J. E: Soft Matter Biol. Phys.* **2000**, *3*, 159–163.

(7) Krupenkin, T.; Yang, S.; Mach, P. *Appl. Phys. Lett.* **2003**, *82*, 316–318.

(8) Murade, C. U.; Oh, J. M.; van den Ende, D.; Mugele, F. *Opt. Express* **2011**, *19*, 15525–15531.

(9) Dzubiella, J.; Hansen, J.-P. *J. Chem. Phys.* **2005**, *122*, 234706.

(10) Smirnov, S. N.; Vlassiouk, I. V.; Lavrik, N. V. *ACS Nano* **2011**, *5*, 7453–7461.

(11) Powell, M. R.; Cleary, L.; Davenport, M.; Shea, K. J.; Siwy, Z. S. *Nat. Nanotechnol.* **2011**, *6*, 798–802.

(12) Santana-Blank, L.; Rodríguez-Santana, E. *Photomed. Laser Surg.* **2010**, *28*, S173–S174.

(13) Santana-Blank, L.; Rodríguez-Santana, E.; Santana-Rodríguez, K. *Photomed. Laser Surg.* **2010**, *28*, S42–S52.

(14) Frank, H. S. *J. Chem. Phys.* **1955**, *23*, 2023.

(15) Striolo, A. *Adsoprt. Sci. Technol.* **2011**, *29*, 211–258.

(16) Daub, C. D.; Bratko, D.; Luzar, A. *Top. Curr. Chem.* **2012**, *307*, 155–180.

(17) Bratko, D.; Daub, C. D.; Leung, K.; Luzar, A. *J. Am. Chem. Soc.* **2007**, *129*, 2504–2510.

(18) Daub, C. D.; Bratko, D.; Leung, K.; Luzar, A. *J. Phys. Chem. C* **2007**, *111*, 505–509.

(19) Bratko, D.; Daub, C. D.; Luzar, A. *Faraday Discuss.* **2009**, *141*, 55–66.

(20) Zhang, X.; Zhu, Y.; Granick, S. *Science* **2002**, *295*, 663–666.

(21) Uchida, K.; Izumi, N.; Sukata, S.; Kojima, Y.; Nakamura, S.; Irie, M. *Angew. Chem., Int. Ed.* **2006**, *45*, 6470–6473.

(22) Lahann, J.; Mitragotri, S.; Tran, T.-N.; Kaido, H.; Sundaram, J.; Choi, I. S.; Hoffer, S.; Somorjai, G. A.; Langer, R. *Science* **2003**, *299*, 371–374.

(23) Lim, H. S.; Han, J. T.; Kwak, D.; Jin, M.; Cho, K. *J. Am. Chem. Soc.* **2006**, *128*, 14458–14459.

(24) Wan, Z.; Zeng, H.; Feinerman, A. *Appl. Phys. Lett.* **2006**, *89*, 201107.

(25) Hsieh, J.; Mach, P.; Cattaneo, F.; Yang, S.; Krupenkine, T.; Baldwin, K.; A., R. J. *IEEE Photonics Technol. Lett.* **2003**, *15*, 81–83.

(26) Daub, C. D.; Bratko, D.; Ali, T.; Luzar, A. *Phys. Rev. Lett.* **2009**, *103*, 207801.

(27) Bonthuis, D. J.; Gekle, S.; Netz, R. R. *Langmuir* **2012**, *28*, 7679–7694.

(28) Werder, T.; Walther, J. H.; Jaffe, R. L.; Halicioglu, T.; Koumoutsakos, P. *J. Phys. Chem. B* **2003**, *107*, 1345–1352.

(29) Wang, J.; Bratko, D.; Luzar, A. *Proc. Natl. Acad. Sci. U. S. A.* **2011**, *108*, 6374–6379.

(30) Hautman, J.; Klein, M. L. *Phys. Rev. Lett.* **1991**, *67*, 1763–1766.

(31) Daub, C. D.; Bratko, D.; Luzar, A. *J. Phys. Chem. C* **2011**, *115*, 22393–22399.

(32) Berendsen, H. J. C.; Grigera, J. R.; Straatsma, T. P. *J. Phys. Chem.* **1987**, *91*, 6269–6271.

(33) Vaitheeswaran, S.; Yin, H.; Rasaiah, J. C. *J. Phys. Chem. B* **2005**, *109*, 6629–6635.

(34) Bratko, D.; Daub, C. D.; Luzar, A. *Phys. Chem. Chem. Phys.* **2008**, *10*, 6807–6813.

(35) Lee, C.; McCammon, J. A.; Rossky, P. J. *J. Chem. Phys.* **1984**, *80*, 4448–4455.

(36) Shelley, J. C.; Patey, G. N. *Mol. Phys.* **1996**, *88*, 385–398.

(37) Yang, K.-L.; Yiacoumi, S.; Tsouris, C. *J. Chem. Phys.* **2002**, *117*, 337.

(38) Song, C.; Wang, P. *Rev. Sci. Instrum.* **2010**, *81*, 054702.

(39) Stillinger, F. H. *The Liquid State of Matter: Fluids Simple and Complex*; North-Holland Publishing Company: Amsterdam, Netherlands, 1982.

(40) Saitta, A. M.; Saija, F.; Giaquinta, P. V. *Phys. Rev. Lett.* **2012**, *108*, 207801.

(41) Stuve, E. M. *Chem. Phys. Lett.* **2012**, *519-520*, 1–17.

(42) Liu, P.; Harder, E.; Berne, B. J. *J. Phys. Chem. B* **2005**, *109*, 2949–2955.

(43) Tainter, C. J.; Pieniazek, P. A.; Lin, Y.-S.; Skinner, J. L. *J. Chem. Phys.* **2011**, *134*, 184501.

(44) Boresch, S.; Steinhauser, O. *Ber. Bunsenges. Phys. Chem.* **1997**, *101*, 1019–1029.

(45) van der Spoel, D.; van Maaren, P. J.; Berendsen, H. J. C. *J. Chem. Phys.* **1998**, *108*, 10220–10230.

(46) Smith, P. E.; van Gunsteren, W. F. *J. Chem. Phys.* **1994**, *100*, 3169–3174.

(47) Svishchev, I. M.; Kusalik, P. G.; Wang, J.; Boyd, R. J. *J. Chem. Phys.* **1996**, *105*, 4742–50.

(48) Zasetsky, A. Y.; Petelina, S. V.; Lyashchenko, A. K.; Lileev, A. S. *J. Chem. Phys.* **2010**, *133*, 134502.

(49) Plimpton, S. *J. Comput. Phys.* **1995**, *117*, 1–19.

(50) Yeh, I.-C..; Berkowitz, M. L. *J. Chem. Phys.* **1999**, *111*, 3155.

(51) Yeh, I.-C..; Berkowitz, M. L. *J. Chem. Phys.* **1999**, *110*, 7935.

(52) Dzubiella, J.; Allen, R. J.; Hansen, J.-P. *J. Chem. Phys.* **2004**, *120*, 5001–5004.

(53) Luzar, A.; Svetina, S.; Žekš, B. *Studia Biophysica* **1982**, *91*, 89–90.

(54) Luzar, A.; Svetina, S.; Žekš, B. *Chem. Phys. Lett.* **1983**, *96*, 485–490.

(55) Stirnemann, G.; Rossky, P. J.; Hynes, J. T.; Laage, D. *Faraday Discuss.* **2010**, *146*, 263–281.

(56) Sutmann, G. *J. Electroanal. Chem.* **1998**, *450*, 289–302.

(57) Schweighofer, K. J.; Benjamin, I. *J. Electroanal. Chem.* **1995**, *391*, 1–10.

(58) Suresh, S. J.; Satish, A. V.; Choudhary, A. *J. Chem. Phys.* **2006**, *124*, 074506.

(59) Suresh, S. J. *J. Chem. Phys.* **2007**, *126*, 2722745.

(60) Kiselev, M.; Heinzinger, K. *J. Chem. Phys.* **1996**, *105*, 650–657.

(61) Maerzke, K. A.; Siepmann, J. I. *J. Phys. Chem. B* **2010**, *114*, 4261–4270.

(62) Errington, J. R.; Debenedetti, P. G. *Nature* **2001**, *409*, 318–321.

(63) Wu, J. Z.; Bratko, D.; Blanch, H. W., Prausnitz, J. M. *J. Chem. Phys.* **1999**, *111*, 7084.

(64) Bratko, D.; Jonsson, B.; Wennerstrom, H. *Chem. Phys. Lett.* **1986**, *128*, 449–454.

(65) Smith, J. D.; Saykally, R. J.; Geissler, P. L. *J. Am. Chem. Soc.* **2007**, *129*, 13847–13856.

(66) Lee, S. H.; Rossky, P. J. *J. Chem. Phys.* **1994**, *100*, 3334–3345.

(67) Zhang, Z.; Berkowitz, M. L. *J. Phys. Chem. B* **2009**, *113*, 7676–7680.

(68) Benjamin, I. *J. Phys. Chem. B* **2005**, *109*, 13711–13715.

(69) Chowdhary, J.; Ladanyi, B. M. *J. Phys. Chem. B* **2008**, *112*, 6259–6273.

(70) Chowdhary, J.; Ladanyi, B. M. *J. Phys. Chem. B* **2009**, *113*, 4045–4053.

(71) Milischuk, A. A.; Ladanyi, B. M. *J. Chem. Phys.* **2011**, *135*, 174709.

(72) Luzar, A.; Chandler, D. *Phys. Rev. Lett.* **1996**, *76*, 928–931.

(73) Saito, S.; Ohmine, I. *J. Chem. Phys.* **1994**, *101*, 6063.

(74) Farrer, R. A.; Fourkas, J. T. *Acc. Chem. Res.* **2003**, *36*, 605–612.

(75) Castrillón, S. R.-V.; Giovambattista, N.; Aksay, I. A.; Debenedetti, P. G. *J. Phys. Chem. B* **2009**, *113*, 1438–1446.

(76) Rønne, C.; Åstrand, P.-O.; Keiding, S. R. *Phys. Rev. Lett.* **1999**, *82*, 2888–2891.

(77) Qiao, W.; Yang, K.; Thoma, A.; Dekorsy, T. *Int. J. Infrared Millimeter Waves* **2012**, *33*, 1029–1038.

(78) Barthel, J.; Bachhuber, K.; Buchner,; Hetzenauer, H. *Chem. Phys. Lett.* **1990**, *165*, 369–373.

(79) Ohmine, I. *J. Phys. Chem.* **1995**, *99*, 6767–6776.

(80) Luzar, A. *J. Chem. Phys.* **2000**, *113*, 10663–10675.

(81) Eaves, J. D.; Loparo, J. J.; Fecko, C. J.; Roberts, S. T.; Tokmakoff, A.; Geissler, P. L. *Proc. Natl. Acad. Sci. U. S. A.* **2005**, *102*, 13019–13022.

Graphical TOC Entry